Electronic Supplementary Material (ESI) for Soft Matter.

Topology of ferroelectric nematic droplets: the case driven by flexoelectricity or depolarization field

Yu Zou,[a] *Jidan Yang ,*[a] *Xinxin Zhang,*[a] *Mingjun Huang* [a,b] *and Satoshi Aya* *[a,b]

[a] South China Advanced Institute for Soft Matter Science and Technology (AISMST), School of Molecular Science and Engineering, South China University of Technology, Guangzhou 510640, China.

[b] Guangdong Provincial Key Laboratory of Functional and Intelligent Hybrid Materials and Devices, South China University of Technology, Guangzhou, 510640, China.

* Corresponding Author. E-mail: satoshiaya@scut.edu.cn (S.A.)

Part I: Supplementary Figure 1

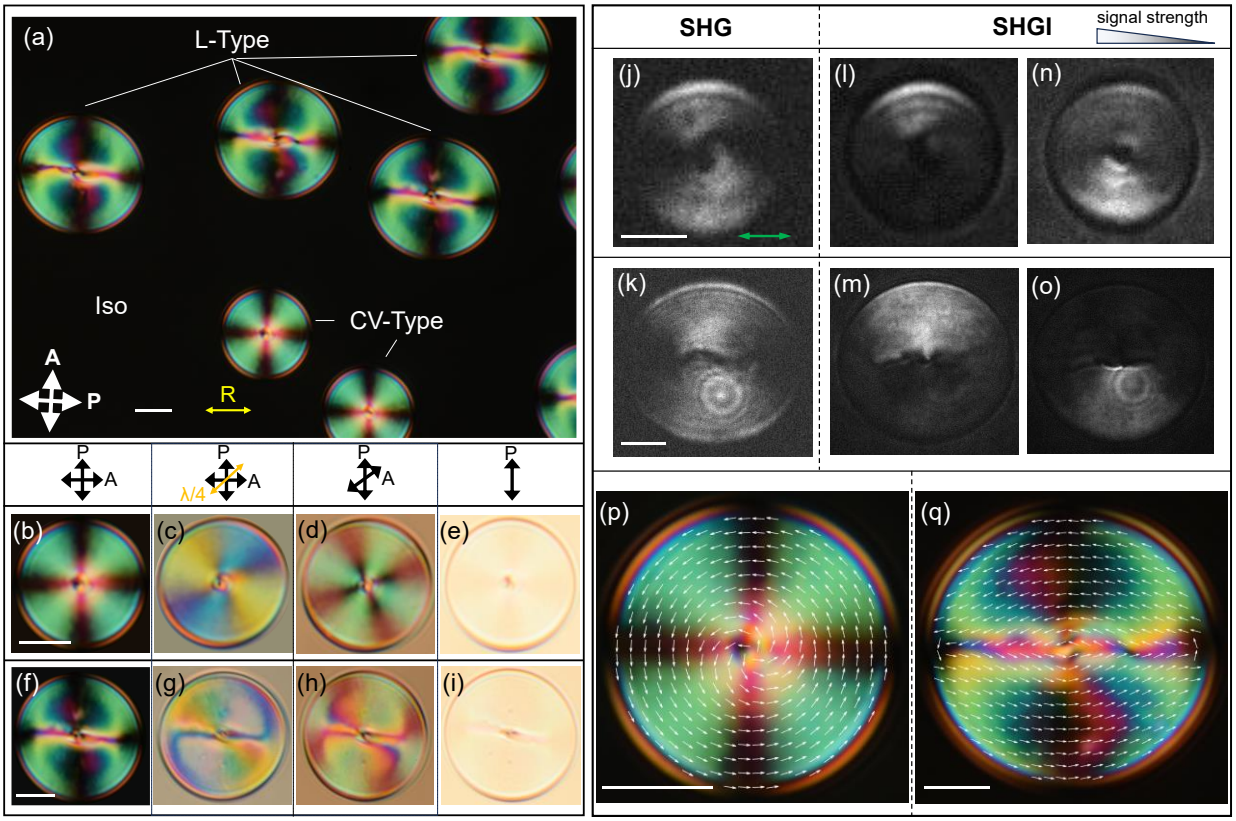

Fig. S1. Polarization textures probed by PLM, SHG, and SHG-I microscopy. (a) The PLM observation of two types of N_F droplets formed by RM-OC_2. The yellow double arrow donates the rubbing direction. (b-e) PLM images of an N_F droplet with the CV-type structure under the crossed polarizers (b), inserting a quarter-wave plate whose slow axis donated by orange double arrows (c), rotating one of the polarizers (d), and removing the analyzer (e). (f-I) PLM images of an N_F droplet with the L-type structure under the crossed polarizers (f), inserting quarter-wave plate (g), rotating one of the polarizers (h), and removing the analyzer (i). (j-n) SHG and SHG-I images of an N_F droplet with CV-type structure. The green double arrow donates the polarization of the laser that excites the SHG or SHG-I signal. (k-o) SHG and SHG-I images of an N_F droplet with L-type polarization topology. Two polarization topologies were reconstructed in N_F droplets: CV-type (p) and L-type (q). Scare bare: 10 μm.

Part II: Reconstruction of the polarization fields

Experimentally, we identified two distinct polarization topologies in pancake-like confined spaces within both RM-OC2 and Nt4 ferroelectric nematic liquid crystal systems (Fig. S1(a)). We initially need to reconstruct the corresponding polarization fields to clarify their topological structures. The polarization structure displays a Maltese-cross pattern at the droplet's periphery during the transition from the isotropic (Iso) state to the ferroelectric nematic state. However, there is no extinction at the droplet's core areas under polarizing light microscopy (PLM) with crossed polarizers (Fig. S1(b)). This implies a distinction in the orientation of the directors in these two areas. Inserting a quarter-wave plate between the crossed polarizers, as illustrated in Fig. S1(c), causes a color change from green to blue in the first and third quadrants (excluding the areas near the center's singularity). This indicates a decrease in optical retardation, suggesting that the orientation of directors in these regions is approximately perpendicular to the slow axis of the quarter-wave plate (yellow double arrows). Conversely, a green-yellow color in the second and fourth quadrants signifies an increase in optical retardation, implying that the orientation of directors is approximately parallel to the slow axis of the quarter-wave plate. Furthermore, by counterclockwise rotation of one of the polarizers, the Maltese-cross pattern at the droplet's periphery rotates in the same direction (Fig. S1(d)), signifying a topological surround number of +1 in the polarization field in this region. Upon removal of one of the polarizers, a singularity is present only in the droplet center (Fig. S1(e)), indicating continuity in the director field elsewhere. Based on the PLM images, the initial director field of the droplet appears to be a concentric vortex-like structure. The core region exhibits a different director orientation than the periphery, with a continuous transition between the two. As the droplet grows, we observe the emergence of another topology (Fig. S1(a) and Figs. S1(f)-(i)). Comparison of PLM images reveals that the directors' orientation in this droplet is similar to the preceding one, except for the area near the topological declination. After inserting the quarter-wave plate, the colors on the two sides of the declination differ significantly (Fig. S1(g)), indicating a difference in directors' orientation between the two sides. Based on the above PLM experimental data, the corresponding director fields for each of the two types of droplets can be reconstructed by using 4×4 matrix method. This method is based on the Berreman's equation, i.e.,

$$\frac{\partial \Psi}{\partial \mathrm{z}} = i\frac{\omega}{c}\Delta_{\mathrm{B}}\Psi. \tag{S1}$$

Ψ represents a vector whose elements are the electric field components (**E**) of light and magnetic field components (**H**) of light, i.e., $\Psi = [E_x, E_y, H_x, H_x]$. ω is the angular frequency of the light. c is the speed of light in a vacuum. Δ_{B} is a 4×4 matrix that contains information about the material's dielectric constant and refractive index, i.e.,

$$\Delta_{\mathrm{B}} = \begin{bmatrix} -K_{xx}\dfrac{\varepsilon_{zx}}{\varepsilon_{zz}} & -K_{xx}\dfrac{\varepsilon_{zy}}{\varepsilon_{zz}} & 0 & 1-\dfrac{{K_{xx}}^2}{\varepsilon_{zz}} \\ 0 & 0 & -1 & 0 \\ \varepsilon_{yz}\dfrac{\varepsilon_{zx}}{\varepsilon_{zz}} - \varepsilon_{yx} & {K_{xx}}^2 - \varepsilon_{yy} + \varepsilon_{yz}\dfrac{\varepsilon_{zy}}{\varepsilon_{zz}} & 0 & K_{xx}\dfrac{\varepsilon_{yz}}{\varepsilon_{zz}} \\ \varepsilon_{xx} - \varepsilon_{xz}\dfrac{\varepsilon_{zx}}{\varepsilon_{zz}} & \varepsilon_{xy} - \varepsilon_{xz}\dfrac{\varepsilon_{zy}}{\varepsilon_{zz}} & 0 & -K_{xx}\dfrac{\varepsilon_{xz}}{\varepsilon_{zz}} \end{bmatrix}. \tag{S2}$$

K_{xx} is defined as $K_{xx} \equiv n_i \sin\theta_i$, where n_i is the refractive index of air (or an ambient), and θ_i shows the angle of incidence. The solution of the Berreman's equation has the form

$$\Psi(d) = \Psi(0)e^{-i\frac{\omega}{c}\Delta_B d}. \quad \text{(S3)}$$

d is the sample thickness. $\Psi(d)$ and $\Psi(0)$ are the tangential components of **E** and **H** of the outgoing and incident light, respectively. In our reconstruction process, we initially derive an initial rough director field through PLM image analysis. Subsequently, we defined the index of refraction n_{ij} and dielectric constant tensor ε_{ij} for the N_F material. The birefringence of the N_F LCs was set to be 0.21 ($n_o = 1.7$ and $n_e = 1.49$). Combined with the director field orientation from the previous step, the index of refraction n_{ij} as well as the dielectric constant tensor ε_{ij} can be calculated for each director (Note that $\varepsilon_{ij} = {n_{ij}}^2$). Then, we defined the light source information. We set the wavelength λ range of the light source to be 380 nm ~ 780 nm, so the corresponding angular frequency ω range is 2.42×10^{15} Hz ~ 4.96×10^{15} Hz (Note that $\omega = 2\pi c/\lambda$). The angle of incidence was set to be $\theta_i = 0$. The sample thickness d is 5 μm. The refractive index of air and LC cells were assumed to be 1 and 1.5, respectively. Substituting the above information into the Berreman's equation, we obtain the transfer matrix $\mathbf{T}_p$ between the incident and the outgoing light, which is

$$\mathbf{T}_p = e^{-i\frac{\omega}{c}\Delta_B d} \quad \text{(S4)}$$

Using Eq. (S4), we calculate the corresponding outgoing light $\Psi(d)$ and subsequently obtain the fitted PLM images. Finally, we iteratively optimize the structure of the director field using the Monte Carlo-simulated annealing algorithm, aligning the fitted PLM image with the actual PLM image. This process results enables us to obtain the director field of the N_F droplet.

Later, both of the aforementioned topological patterns in the NF droplets manifest as polarization structures, as evidenced by second harmonic generation (SHG) microscopic images (Figs. S1(j) and (k)). Figs. S1(l)-(o) depict the SHG images of the CV- and L-type droplets under two interference conditions, where the phase of the SH signal of a reference quartz plate is shifted by π. The SH signal alternates between the upper and lower parts of the two types of droplets, indicating a reversal in the polarization orientation of these two halves. Combining these SHG experimental data then allows us to derive the final polarization structures (Figs. S1(p) and (q)).

Part III: Modelling of 2D polarization fields

We establish the mathematical expressions for the 2D polarization fields of the CV-type and the L-type structures according to the reconstruction results in Figs. S1(p) and (q). The director field is represented by a unit vector of $\mathbf{n} = (\cos\varphi\cos\psi, \sin\varphi\cos\psi, \sin\psi)$. φ and ψ are the azimuth and elevation angles for the director.

The director field of the CV-type structure is modeled by using

$$\varphi = \theta + kr + b, \quad \text{(S5)}$$
$$\psi = 0. \quad \text{(S6)}$$

θ and r are the polar angle and radius in the polar coordinate system with the origin point located in the droplet center, respectively. k represents the variation rate of the azimuth angle along the droplet's radius.

b represents the initial azimuth angle at the center of the droplet. Thus, the expression of the director field in the Cartesian coordinate system is expressed as

$$n_x = \frac{x\cos\left(k\sqrt{x^2+y^2}+b\right) - y\sin\left(k\sqrt{x^2+y^2}+b\right)}{\sqrt{x^2+y^2}}, \tag{S7}$$

$$n_y = \frac{y\cos\left(k\sqrt{x^2+y^2}+b\right) + x\sin\left(k\sqrt{x^2+y^2}+b\right)}{\sqrt{x^2+y^2}}, \tag{S8}$$

$$n_z = 0. \tag{S9}$$

Setting $k \neq 0$ in Eqs. (S7 − S9) enables the description of the splay deformation in the inner part of the CV-type structure observed experimentally. When $k = 0$ and $b = \pi/2$ in Eqs. (S7 − S9), the concentric polarization field at the periphery part is described (Fig. 1(n)).

For The L-type structure, the model is also divided into two areas: the inner and the periphery parts. In the inner part, we set the azimuth and elevation angles as

$$\varphi = \begin{cases} \tan^{-1}\dfrac{-xy}{L^2} & \text{if } y > 0 \\ \tan^{-1}\dfrac{-xy}{L^2} + \pi & \text{if } y < 0 \end{cases}, \tag{S10}$$

$$\psi = 0. \tag{S11}$$

L donates the inner radius of the L-type droplet, which is comparable with the length of the line disclination. The spatial distribution of the director in the inner part is written as

$$n_x = \frac{yL^2}{|y|\sqrt{L^4+x^2y^2}}, \tag{S12}$$

$$n_y = \frac{-xy^2}{|y|\sqrt{L^4+x^2y^2}}, \tag{S13}$$

$$n_z = 0. \tag{S14}$$

The concentric polarization field in the periphery part is consistent with that in the CV-type structure, described by Eqs. (S7 − S9), where $k = 0$ and $b = \pi/2$.

Due to the dominant role of the dipolar interaction driving the polar nematic order in rod-shaped N_F systems, our compounds undergo a direct Iso-N_F transition without transitioning into apolar nematics as temperature decreases. In this scenario, the nematic order is induced by the polarization order. To explain this, we propose a linear coupling between the nematic order parameter and the polarization order as: $\mathbf{N} = s\mathbf{n}$ and $\mathbf{P} = P_0\mathbf{N} = P_0 s\mathbf{n}$ [1]. s is the scalar order parameter for the uniaxial case. P_0 is the maximum polarization intensity when a perfect order (i.e., $s = 1$) is achieved. The polarization fields for CV- and L-type structures can be modeled as shown in Figs. 1(n,o).

Part IV: Free-energy calculation for the CV-type structure

In our model, the free energy density functional consists of a bulk term f_{b} and a surface term f_{s}. They are

$$f_{\mathrm{bulk}} = \frac{K_{11}(\nabla \cdot \mathbf{N})^2}{2} + \frac{K_{22}[\mathbf{N} \cdot (\nabla \times \mathbf{N})]^2}{2} + \frac{K_{33}[\mathbf{N} \times (\nabla \times \mathbf{N})]^2}{2} + \frac{\tau_1 \mathbf{P}^2}{2} + \frac{\tau_2 \mathbf{P}^4}{2} + \frac{h(\nabla \mathbf{P})^2}{2} - \gamma \mathbf{N}(\nabla \cdot \mathbf{N}) \cdot \mathbf{P} - \frac{1}{2}\mathbf{P} \cdot \mathbf{E}_{\mathrm{d}}, \quad \text{(S15)}$$

$$f_{\mathrm{surf}} = \frac{1}{2} W_{\mathrm{Q}}[1 - (\mathbf{n} \cdot \mathbf{n}_0)^2] - W_{\mathrm{P}}(\mathbf{n} \cdot \mathbf{n}_0 - 1). \quad \text{(S16)}$$

The first three terms in Eq. (S15) are the nematic elastic energy density for splay (K_{11}), twist (K_{22}), and bend (K_{33}) deformations. The fourth and fifth terms represent the Landau energy for realizing a polar phase. $\tau_1 = \alpha(T - T_0)$ and τ_2 are the phenomenological coefficients. T_0 is the critical temperature for the apolar-polar phase transition. The equilibrium polarization of the system is $\mathbf{P}_0 = s_0 P_0 \mathbf{n}$, whose magnitude is determined by the Landau coefficients, i.e.,$|\mathbf{P}_0| = \sqrt{-\tau_1/(2\tau_2)}$. Note that we only consider the N_F state in equilibrium ($\mathbf{P} = \mathbf{P}_0$), so the Landau energy density here can be simplified as:

$$f_{\mathrm{Lau}} = \frac{\tau_1(\mathbf{P}_0)^2}{2} + \frac{\tau_2(\mathbf{P}_0)^4}{2} = \frac{-{\tau_1}^2}{8\tau_2}. \quad \text{(S17)}$$

The sixth term is the polarization gradient energy density, in which

$$\nabla \mathbf{P} = P_0 \nabla(s\mathbf{n}) = sP_0 \begin{pmatrix} \frac{\partial n_x}{\partial x} & \frac{\partial n_x}{\partial y} & \frac{\partial n_x}{\partial z} \\ \frac{\partial n_y}{\partial x} & \frac{\partial n_y}{\partial y} & \frac{\partial n_y}{\partial z} \\ \frac{\partial n_z}{\partial x} & \frac{\partial n_z}{\partial y} & \frac{\partial n_z}{\partial z} \end{pmatrix}. \quad \text{(S18)}$$

Here, we assumed that the order parameter is spatially homogeneous s ($\nabla s = 0$). The polarization gradient term penalizes any deformation of the polarization field and effectively distinguishes between the ferroelectric and antiferroelectric states [1, 2]. The seventh bulk term deals with flexoelectric polarization which comes from the LC flexoelectric effect. In the N_F state, the flexoelectric polarization couples with the spontaneous polarization field, resulting in the effective splay elastic modulus K_{11} being reduced. γ is a bare flexoelectric coefficient. The last bulk term originates from the depolarization effect. $\mathbf{E}_{\mathrm{d}}$ is the depolarization field in the bulk of the N_F droplet. Electrostatic interactions are particularly significant in the highly polar N_F system at low temperatures. An example is the calculation of the depolarization energy in the core region of a CV-type structure. The polarization field in the N_F droplet produces depolarization charges. The charge density can be calculated as:

$$\rho_{\mathrm{b}} = -\beta(\nabla \cdot \mathbf{P}) = \beta P_{\mathrm{eff}} \left[k\sin(b + kr) - \frac{\cos(b + kr)}{r} \right] \quad \text{(S19)}$$

P_{eff} is regard as the effective polarization strength for the system, i.e., $P_{\mathrm{eff}} = sP_0$. β is a dimensionless coefficient. The actual amount of space charge would be (much) lower than the theoretical prediction due to the existence of free ions [3]. β is set to be of the order of 10^{-4} to calculate the actual space charge density in our N_F droplets. By solving Poisson's equation ($\nabla^2 \Phi = -\rho_{\mathrm{b}}/\varepsilon$), we can further derive the depolarization potential Φ and electric field $\mathbf{E}$, which are:

$$\Phi = C_1 + C_2 \ln r + \frac{\beta P_{\text{eff}} \sin(b + kr)}{k\varepsilon} \tag{S20}$$

$$\mathbf{E} = -\nabla\Phi = \begin{pmatrix} -\dfrac{x[\varepsilon C_2 + \beta P_{\text{eff}} r\cos(b + kr)]}{\varepsilon r^2} \\ -\dfrac{y[\varepsilon C_2 + \beta P_{\text{eff}} r\cos(b + kr)]}{\varepsilon r^2} \\ 0 \end{pmatrix} \tag{S21}$$

ε is the effective dielectric constant of the LC material. C_1 and C_2 are the coefficients from the process of solving the equations. C_1 represents an offset of the potential and C_2 represents a background electric field. Correspondingly, the depolarization energy density for the core regions of a CV-type structure is

$$f_{\text{depol}} = \frac{1}{2} P_{\text{eff}} \cos(b + kr) \left[\frac{C_2}{r} + \frac{\beta P_{\text{eff}} \cos(b + kr)}{\varepsilon} \right]. \tag{S22}$$

For generality, we include two types of anchoring effects from the surface-rubbed LC cells: traditional apolar anchoring and an additional polar anchoring (Eq. (S16)). The apolar anchoring prefers the director either syn-parallel or antiparallel to the rubbing direction. The polar anchoring, on the other hand, favours the polarization only syn-parallel to the rubbing direction. We set the polar anchoring direction to be $\mathbf{n}_0 = (1,0,0)$ here. The magnitude of the apolar and polar anchoring at the cells' surface are controlled by W_{Q} and W_{P}, respectively.

The total free energy of the CV-type structure is calculated by adding up the free energies arising from the inner and periphery parts. In the inner part, the free energy is calculated as

$$\begin{aligned} F_{\text{c}} &= \int_0^{2\pi} \int_a^{R_1} (f_{\text{bulk}} + f_{\text{surf}})|_{k\neq 0} \cdot r \, \mathrm{d}r \, \mathrm{d}\theta \\ &= \frac{\pi\left(\overline{K} + h{P_{\text{eff}}}^2\right)}{2} \left(k^2 {R_1}^2 + 2\ln\frac{R_1}{a} \right) + \pi\widetilde{K}\chi - \frac{\pi{\tau_1}^2}{8\tau_2} {R_1}^2 \\ &\quad -2\pi\gamma P_{\text{eff}} R_1 \cos(b + kR_1) + \frac{\pi}{4}\left(W_{\text{Q}} + 2W_{\text{P}}\right){R_1}^2 \\ &\quad + \frac{\pi\beta {P_{\text{eff}}}^2}{4k^2\varepsilon}\left[k^2 {R_1}^2 + kR_1 \sin(2b + 2kR_1) - \sin(kR_1)\sin(2b + kR_1) \right] \end{aligned} \tag{S23}$$

$$\chi = \int_{2ka}^{2kR_1} \frac{\cos(t + 2b)}{t} \mathrm{d}t - \frac{kR_1}{2}\sin(2b + 2kR_1) - \frac{3}{2}\sin(2b + kR_1)\sin(kR_1) \tag{S24}$$

Note that Eqs. (S7 − S9) fail to describe the polarization field at the center of the droplet due to $\sqrt{x^2 + y^2} = 0$, so we set the radius of this mathematical singularity to be a to avoid divergence of the energy. R_1 is the radius of the core region for the CV-type droplet. $\overline{K}$ is defined as $\overline{K} = (s^2 K_{11} + s^4 K_{33})/2$. The elastic anisotropy is represented by the second term of F_{CV}, where $\widetilde{K} = (s^2 K_{11} - s^4 K_{33})/2$. In addition, we consider the polar anchoring effect very weak for the inner part of the droplets so that $W_{\text{P}} = 0$ in Eq. (S27). In the periphery part of CV-type droplets, an idealized concentric polarization field forms, whose free energy is calculated as

$$F_{\mathrm{p}} = \int_0^{2\pi}\int_{R_1}^{R} (f_{\mathrm{b}} + f_{\mathrm{s}})|_{k=0,b=\frac{\pi}{2}} \cdot r \,\mathrm{d}r \,\mathrm{d}\theta$$
$$= \pi\left(s^4 K_{33} + hP_{\mathrm{eff}}{}^2\right)\ln\frac{R}{R_1} - \frac{\pi\tau_1{}^2}{8\tau_2}\left(R^2 - R_1{}^2\right) + \frac{\pi}{4}\left(W_{\mathrm{Q}} + 2W_{\mathrm{P}}\right)\left(R^2 - R_1{}^2\right) \quad \text{(S25)}$$

Therefore, the total free energy of a CV-type droplet reads

$$F_{\mathrm{CV}} = \frac{\pi}{2}\left(\overline{K} + hP_{\mathrm{eff}}{}^2\right)\left(k^2 R_1{}^2 + 2\ln\frac{R}{a}\right) + \pi\widetilde{K}\left(\chi - \ln\frac{R}{R_1}\right) - \frac{\pi\tau_1{}^2}{8\tau_2}R^2$$
$$-2\pi\gamma P_{\mathrm{eff}} R_1 \cos(b + kR_1) + \frac{\pi}{4}W_{\mathrm{Q}}R^2 + \frac{\pi}{2}W_{\mathrm{P}}\left(R^2 - R_1{}^2\right)$$
$$+\frac{\pi\beta P_{\mathrm{eff}}{}^2}{4k^2\varepsilon}\left[k^2 R_1{}^2 + kR_1\sin(2b + 2kR_1) - \sin(kR_1)\sin(2b + kR_1)\right] \quad \text{(S26)}$$

To simplify the above free energy form, we first try to determine the value of the parameter b, corresponding to the optimal azimuth angle of the polarization near the center of the CV-type structure. Considering the case of $R_1 \approx a \to 0$, the free energy of the CV-type structure is simplified as

$$F_{\mathrm{CVt}} \approx \pi\left(\overline{K} + hP_{\mathrm{eff}}{}^2\right)\ln\frac{R}{a} - \pi\widetilde{K}\left[2\sin(2b)kR_1 + \ln\frac{R}{R_1}\right]$$
$$-2\pi\gamma P_{\mathrm{eff}} R_1 \cos b\,. \quad \text{(S27)}$$

We used some approximation as: e.g., $k^2 R_1{}^2 \sim 0$, $R^2 \sim 0$ and $b + kR_1 \sim b$. The terms related to parameter b are elastic anisotropy and flexoelectricity, i.e.,

$$g(b) = -2\pi\widetilde{K}\sin(2b)kR_1 - 2\pi\gamma P_{\mathrm{eff}} R_1 \cos b\,. \quad \text{(S28)}$$

When $\widetilde{K} \le 0$, the free energy F_{CVt} minimizes when $b = 0$. If $\widetilde{K} > 0$, the optimal parameter b_0 corresponding to the minimization of the function $g(b)$ can be derived by solving

$$\frac{\partial g(b)}{\partial b} = -2\pi R_1\left(2k\widetilde{K}\sin 2b_0 - \gamma P_{\mathrm{eff}}\cos b_0\right) = 0. \quad \text{(S29)}$$

Then, the optimal parameter b_0 becomes

$$b_0 = \sin^{-1}\frac{\sqrt{\varsigma^2 + 32} - \varsigma}{8}. \quad \text{(S30)}$$

Here, ς is the radio of flexoelectricity and the elastic anisotropic, i.e., $\varsigma = \gamma P_{\mathrm{eff}}/k\widetilde{K}$. Worth noting that the values of b_0 can go to zero when the flexoelectric effect is dominant (i.e., $\gamma P_0 \gg \widetilde{K}$). This situation may easily occur at the initial stage of the Iso-N_F transition. Based on the above discussion and for convenience, we will consider $b = 0$ in the following calculation. We then applied this condition to Eq. (S26).

To investigate the optimal CV-type structure, we calculated the equilibrium inner radius $R_{\mathrm{e}1}$ for the CV-type droplet. We first calculate the first-order partial derivatives of F_{CV} with respect to R_1, which gives an equation for $R_{\mathrm{e}1}$:

$$\frac{\partial F_{\mathrm{CV}}}{\partial R_1} = 0 \Rightarrow$$
$$\widetilde{K}[1 + \cos 2\phi_0 - 2kR_{\mathrm{e}1}\sin 2\phi_0 - (kR_{\mathrm{e}1})^2\cos 2\phi_0] + \frac{\beta P_{\mathrm{eff}}{}^2}{\varepsilon}R_{\mathrm{e}1}{}^2\cos^2\phi_0$$
$$= 2\gamma P_{\mathrm{eff}} R_{\mathrm{e}1}(\cos\phi_0 - kR_{\mathrm{e}1}\sin\phi_0) - \left[k^2\left(\overline{K} + hP_{\mathrm{eff}}{}^2\right) - W_{\mathrm{P}}\right]R_{\mathrm{e}1}{}^2. \quad \text{(S31)}$$

ϕ_0 is set to be $\phi_0 = b + kR_{e1}$, which represents the azimuth angle of the polarization on the boundary of the core area. The range of values of ϕ_0 is $(0, \pi/2)$. The trigonometric terms in Eq. (S35) can therefore be handled by course-grained method for simplification, e.g., $\langle \cos 2\phi_0 \rangle = 0$, $\langle \sin 2\phi_0 \rangle = 1$, $\langle \cos^2 \phi_0 \rangle = 1/2$ and $\langle \cos \phi_0 \rangle = \langle \sin \phi_0 \rangle = 2/\pi$. So, we obtained the solution for the equilibrium inner radius R_{e1} as

$$R_{e1} \approx \frac{4\eta + \sqrt{16\eta^2 - 2\pi\widetilde{K}\zeta}}{\zeta}, \tag{S32}$$

$$\zeta = 2\pi k^2\left(\overline{K} + hP_{\text{eff}}{}^2\right) + 8k\gamma P_0 + \pi\frac{\beta P_{\text{eff}}{}^2}{\epsilon} - \pi W_{\text{P}}, \tag{S33}$$

$$\eta = \gamma P_{\text{eff}} + k\widetilde{K}. \tag{S34}$$

We briefly discuss how the elastic anisotropy affects the equilibrium CV-type structure based on Eqs. $(S32 - S34)$. Taking the first-order partial derivatives of R_{e1} with respect to $\widetilde{K}$, we obtained

$$\frac{\partial R_{e1}}{\partial \widetilde{K}} = \frac{2[3(2kR_{e1} - \pi) + 8k(1 - k\eta)]}{\zeta\sqrt{16\eta^2 - 2\pi\widetilde{K}\zeta}}. \tag{S35}$$

Since kR_{e1} ranges in value from $(0, \pi/2)$ as discussed earlier and $k\eta < 1$ is known after substituting numerical values (e.g., $k = \pi/10$ μm^{-1}, $\gamma = 10^{-4}$ V, $P_{\text{eff}} = 4.5$ μC·cm^{-2}), R_{e1} decreases as $\widetilde{K}$ increases. Physically, different ferroelectric LCs may exhibit either positive [4] or negative [5] values of $\widetilde{K}$. If $\widetilde{K} < 0$, the effective splay elastic modulus is smaller than the effective bend elastic modulus K_{33}, suggesting that the elastic anisotropy favors expanding the inner radius of the CV-type structure. If $\widetilde{K} > 0$, the effective splay modulus K_{11} is larger than the effective bend modulus K_{33}, implying that the elastic anisotropy suppresses the expansion of the inner areas in the CV-type structure. A similar scenario that the condition of $K_{33}/(8K_{11}) + K_{22}/K_{11} \leq 1$ in apolar N droplets leads to the called twisted radial structure (an apolar analogy of the vortex-like topology) under the homeotropic anchoring. This is because the radial configuration is unstable against a twist deformation as K_{33} decreases. In the N_F droplets, the elastic anisotropy does not affect the essence of the formation of polarization topology (Fig. 2), so we further simplify the equilibrium inner radius under the single-elastic-constant approximation as:

$$R_{e1} \approx \frac{8\gamma P_{\text{eff}}}{2\pi k^2\left(\overline{K} + hP_{\text{eff}}{}^2\right) + 8k\gamma P_{\text{eff}} + \frac{\pi\beta P_{\text{eff}}{}^2}{\varepsilon} - \pi W_{\text{P}}}. \tag{S36}$$

Correspondingly, the free energy of an CV-type droplet with an equilibrium inner diameter R_{e1} is

$$\begin{aligned} F_{\text{CVe}} \approx{}& \pi\left(\overline{K} + hP_{\text{eff}}{}^2\right)\left[\frac{k^2 R_{e1}{}^2}{2} + \ln\frac{R}{a}\right] - \frac{\pi\tau_1{}^2}{8\tau_2}R^2 - 2\pi\gamma P_{\text{eff}}R_{e1}\cos(kR_{e1}) \\ &+ \frac{\pi}{4}W_{\text{Q}}R^2 + \frac{\pi}{2}W_{\text{P}}\left(R^2 - R_{e1}{}^2\right) + \frac{\pi\beta P_{\text{eff}}{}^2}{4k^2\varepsilon}[k^2 R_{e1}{}^2 + \\ &kR_{e1}\sin(2b + 2kR_{e1}) - \sin(kR_{e1})\sin(2b + kR_{e1})] \end{aligned} \tag{S37}$$

Using Eq. (S31), we can further simplify Eq. (S37) as

$$F_{\text{CVe}} \approx \pi\left(\overline{K} + hP_{\text{eff}}{}^2\right)\ln\frac{R}{a} - \frac{\pi\tau_1{}^2}{8\tau_2}R^2 + \frac{\beta P_{\text{eff}}{}^2}{4\varepsilon}R_{e1} + \frac{\pi}{4}\left(W_{\text{Q}} + 2W_{\text{P}}\right)R^2 \tag{S38}$$

Part V: Free-energy calculation for the L-type structure

The total free energy of an L-type droplet is calculated by adding up three parts. First, the polarization field in its core area can be described by Eq. (S12 − S14), and this region is considered a circular shape with a radius of L. According to Eq. (S15 − S16), the corresponding free energy density is calculated as:

$$f_{\mathrm{ela}} = \frac{s^2 K_{11}}{2L^2} \cdot \frac{x'^2\left(1+y'^2\right)^2}{\left(1+x'^2y'^2\right)^3} + \frac{s^4 K_{33}}{2L^2} \cdot \frac{y'^2\left(1-x'^2\right)^2}{\left(1+x'^2y'^2\right)^3} \tag{S39}$$

$$f_{\mathrm{Lau}} = \frac{-{\tau_1}^2}{8\tau_2} \tag{S40}$$

$$f_{\mathrm{grad}} = \frac{h{P_{\mathrm{eff}}}^2}{2L^2} \cdot \frac{x'^2+y'^2}{\left(1+x'^2y'^2\right)^3} \tag{S41}$$

$$f_{\mathrm{flexo}} = \frac{\gamma P_{\mathrm{eff}}}{L} \cdot \frac{x'\left(1+y'^2\right)}{\left(1+x'^2y'^2\right)^{\frac{3}{2}}} \tag{S42}$$

$$f_{\mathrm{surf}} = \frac{W_{\mathrm{Q}}}{2} \cdot \frac{x'^2y'^2}{1+x'^2y'^2} \tag{S43}$$

We define $x' = x/L$ and $y' = y/L$, and they take values in the range of $[-1,1]$. The depolarization charges induced by the L-type structure is calculated as:

$$\begin{aligned} \rho_{\mathrm{b}} &= -\beta(\nabla \cdot \mathbf{P}) \\ &= \frac{\beta P_{\mathrm{eff}}}{L} \cdot \frac{x'\left(1+y'^2\right)}{\left(1+x'^2y'^2\right)^{\frac{3}{2}}} \end{aligned} \tag{S44}$$

After substituting Eq. (S44) into Poisson's equation, a non-homogeneous second-order differential equation is obtained. Because it is difficult to obtain analytical solutions, we conducted numerical calculations. Firstly, we numerically solve the equation of

$$\nabla^2\Phi_1 = -\frac{x'\left(1+y'^2\right)}{\left(1+x'^2y'^2\right)^{\frac{3}{2}}} \tag{S45}$$

in a grid space of size $[x', y'] \in [-1,1]$ with a step length of 0.01 μm. A solution of Φ_1 with numerical-matrix type was obtained. Then, we numerically solve the corresponding depolarization field through the equation of $\mathbf{E}_1 = -\nabla\Phi_1$. We considered a L-type structure ($\mathbf{P'} = (P'_{x'}, P'_{y'}, P'_{z'})$) as

$$P'_{x'} = \frac{P_{\mathrm{eff}}y'}{|y'|\sqrt{1+x'^2y'^2}}, \tag{S46}$$

$$P'_{y'} = \frac{-P_{\mathrm{eff}}x'y'^2}{|y'|\sqrt{1+x'^2y'^2}}, \tag{S47}$$

$$P'_{z'} = 0. \tag{S48}$$

So, the depolarization energy density in the grid space can be calculated by the equation of

$$f'_{\mathrm{depol}} = -\frac{1}{2}\mathbf{P}' \cdot \mathbf{E}_1 \tag{S49}$$

f'_{depol} is a numerical matrix. We denote the average value of f'_{depol} as N_1, and then the actual depolarization energy density of an L-type structure with a radius of L can be estimated as

$$f_{\mathrm{depol}} = \frac{\beta P_{\mathrm{eff}}}{L} f'_{\mathrm{depol}} \approx N_1 \frac{\beta P_{\mathrm{eff}}}{L} \tag{S50}$$

Finally, we perform a numerical integration in the region of $x'^2 + y'^2 < 1$ to obtain the free energy of the inner part of an L-type droplet, the results are

$$\begin{aligned} F_L &= L^2 \int_{-1}^{1} \int_{-\sqrt{1-x'^2}}^{\sqrt{1-x'^2}} (f_{\mathrm{bulk}} + f_{\mathrm{surf}})\, \mathrm{d}y'\, \mathrm{d}x' \\ &\approx 0.45 s^2 K_{11} + 0.25 s^4 K_{33} - \frac{\pi {\tau_1}^2}{8\tau_2} L^2 + 0.70 h {P_{\mathrm{eff}}}^2 + N_1 \frac{\pi \beta {P_{\mathrm{eff}}}^2}{\varepsilon} L + 0.06 W_{\mathrm{Q}} L^2. \end{aligned} \tag{S51}$$

The second part of the total free energy is caused by the line disclination in L-type droplets, whose energy is controlled by the nematic elasticity and length, i.e.,

$$F_{\mathrm{d}} = \kappa \bar{K} L. \tag{S52}$$

κ is a constant related to the tension of the line disclination in nematic. The last part of the total free energy is caused by the elastic energy arising from the concentric structure formed in the peripheral area, which is solved as

$$\begin{aligned} F_{\mathrm{p}} &= \int_0^{2\pi} \int_L^R (f_{\mathrm{b}} + f_{\mathrm{s}})|_{k=0, b=\frac{\pi}{2}} \cdot r\, \mathrm{d}r\, \mathrm{d}\theta, \\ &= \pi\left(s^4 K_{33} + h {P_0}^2\right) \ln\frac{R}{L} - \frac{\pi {\tau_1}^2}{8\tau_2}(R^2 - L^2) \\ &+ \frac{\pi\left(W_{\mathrm{Q}} + 4W_{\mathrm{P}}\right)}{4}(R^2 - L^2). \end{aligned} \tag{S53}$$

Therefore, the total free energy of an L-type droplet reads:

$$\begin{aligned} F_{\mathrm{L}} &= 0.45 s^2 K_{11} + s^4 K_{33}\left(0.25 + \pi \ln\frac{R}{L}\right) - \frac{\pi {\tau_1}^2}{8\tau_2} R^2 + \kappa \bar{K} L + N_1 \frac{\pi \beta {P_{\mathrm{eff}}}^2}{\varepsilon} L \\ &+ h {P_{\mathrm{eff}}}^2 \left(0.70 + \pi \ln\frac{R}{L}\right) + \pi W_{\mathrm{P}}(R^2 - L^2) + \frac{\pi}{4} W_{\mathrm{Q}}(R^2 - 0.92 L^2). \end{aligned} \tag{S54}$$

Numerically calculating F_{L} as a function of L under the cases of the single-elastic-constant approximation and the three-elastic-constant condition are shown in Fig. 3. The landscapes of the free energy in both cases are similar. For simplicity of the analytical solution, we consider the single-elastic-constant approximation and obtain

$$F_{\mathrm{L}} = \left(\overline{K} + hP_{\mathrm{eff}}{}^2\right)\left(0.70 + \pi \ln\frac{R}{L}\right) - \frac{\pi {\tau_1}^2}{8\tau_2}R^2 + \kappa \overline{K} L$$
$$+ N_1 \frac{\pi\beta P_{\mathrm{eff}}{}^2}{\varepsilon} L + \frac{\pi}{2} W_{\mathrm{P}}(R^2 - L^2) + \frac{\pi}{4} W_{\mathrm{Q}}(R^2 - 0.92L^2). \quad \text{(S55)}$$

We took the first-order partial derivatives of F_{L} with respect to L, which optimize of the length of the line disclination L_{e} as

$$\frac{\partial F_{\mathrm{L}}}{\partial L} = 0 \Rightarrow$$
$$\pi\left(0.23W_{\mathrm{Q}} + \frac{W_{\mathrm{P}}}{2}\right) {L_{\mathrm{e}}}^2 = \frac{L_{\mathrm{e}}}{2}\left(\kappa\overline{K} + N_1 \frac{\pi\beta P_{\mathrm{eff}}{}^2}{\varepsilon}\right) - \frac{\pi}{2}\left(\overline{K} + hP_{\mathrm{eff}}{}^2\right), \quad \text{(S56)}$$

$$L_{\mathrm{e}} = \frac{\varrho - \sqrt{\varrho^2 - 2\pi W\left(\overline{K} + hP_{\mathrm{eff}}{}^2\right)}}{W}. \quad \text{(S57)}$$

$$\varrho = \kappa\overline{K} + N_1 \frac{\pi\beta P_{\mathrm{eff}}{}^2}{\varepsilon} \quad \text{(S58)}$$

The total anchoring strength is represented by $W = 4\pi\left(0.23W_{\mathrm{Q}} + W_{\mathrm{P}}\right)$, which has to meet $W < \varrho^2/2\pi\left(\overline{K} + hP_0{}^2\right)$. The stronger anchoring out of the range leads the polarization to orient parallel to the rubbing direction, destabilizing the L-type structure. Under this constraint, we took first-order partial derivatives of L_{e} with respect to W, which can deduce that

$$\frac{\partial L_{\mathrm{e}}}{\partial W} = \frac{\pi\left(\overline{K} + hP_{\mathrm{eff}}{}^2\right)}{W\sqrt{\varrho^2 - 2\pi W\left(\overline{K} + hP_{\mathrm{eff}}{}^2\right)}} - \frac{\varrho - \sqrt{\varrho^2 - 2\pi W\left(\overline{K} + hP_{\mathrm{eff}}{}^2\right)}}{W^2}$$
$$\geq \frac{1}{W}\left(\sqrt{\frac{2\varrho^2}{W^2}} - \frac{\varrho}{W}\right) > 0. \quad \text{(S59)}$$

Therefore, we conclude that L_{e} increases with increasing the anchoring strength. Finally, we insert Eq. (56) into Eq. (55) to obtain the free energy of an L-type droplet with the equilibrium defect length L_{e}, which reads:

$$F_{\mathrm{Le}} = \left(\overline{K} + hP_{\mathrm{eff}}{}^2\right)\left(2.27 + \pi \ln\frac{R}{L_{\mathrm{e}}}\right) - \frac{\pi {\tau_1}^2}{8\tau_2}R^2 + \kappa\overline{K}\frac{L_{\mathrm{e}}}{2}$$
$$+ \frac{\pi}{4}\left(W_{\mathrm{Q}} + 2W_{\mathrm{P}}\right)R^2. \quad \text{(S60)}$$

Part VI: Free-energy comparison between the CV- and L-type structures

Comparing Eqs. (S38) and (S60), we can calculate the difference in the free energy for the optimized CV-type and L-type droplets with a certain size, i.e.,

$$\begin{aligned}\Delta F &= F_{\mathrm{Le}} - F_{\mathrm{CVe}} \\ &= \left(\overline{K} + hP_{\mathrm{eff}}{}^2\right)\left(2.27 - \pi \ln \frac{L_{\mathrm{e}}}{a}\right) + \frac{L_{\mathrm{e}}}{2}\left(\kappa \overline{K} - \frac{\beta P_{\mathrm{eff}}{}^2}{2N\varepsilon}\right).\end{aligned} \tag{S61}$$

N is defined as the radio of L_{e} and $R_{\mathrm{e}1}$, i.e., $N = L_{\mathrm{e}}/R_{\mathrm{e}1}$. The condition for the spontaneous transition from the CV- to the L- structure is $\Delta F < 0$. So next, we calculate the critical value $L_{\mathrm{e}0}$ for $\Delta F = 0$. The equation for $L_{\mathrm{e}0}$ is

$$\frac{\left(\overline{K} + hP_{\mathrm{eff}}{}^2\right)}{a} = \frac{\left(\kappa \overline{K} - \frac{\beta P_{\mathrm{eff}}{}^2}{2N\varepsilon}\right)\frac{L_{\mathrm{e}0}}{a}}{2\left(\pi \ln \frac{L_{\mathrm{e}0}}{a} - 2.27\right)} \approx \frac{\left(\kappa \overline{K} - \frac{\beta P_{\mathrm{eff}}{}^2}{2N\varepsilon}\right)a}{2\pi L_{\mathrm{e}0}} \tag{S62}$$

Note that the above equation is valid only when $L_{\mathrm{e}0}/a$ is large. Thus, the critical size of L_{e} for $\Delta F = 0$ is

$$L_{\mathrm{e}0} \approx \frac{a^2}{2\pi\left(\overline{K} + hP_{\mathrm{eff}}{}^2\right)}\left(\kappa \overline{K} - \frac{\beta P_{\mathrm{eff}}{}^2}{2N\varepsilon}\right). \tag{S63}$$

Furthermore, we discussed earlier that L_{e} would increase with the increase of the effective polarization P_{eff}, so there would be a corresponding critical value for P_{eff} to realize $\Delta F < 0$. Combining Eqs. (S60) and (S66), we obtain

$$(1 + h\lambda^2) \approx \frac{a^2(\kappa - \beta/2N\epsilon)^2}{4\pi^2}\left[1 - \frac{2a^2 W}{\pi\left(K + hP_{\mathrm{eff}}{}^2\right)}\right] \tag{S64}$$

λ is a scaled parameter between the polarization strength and the elasticity modulus, i.e., $\lambda = P_{\mathrm{eff}}{}^2/K$. Because a is very small, we obtain the critical λ that makes $\Delta F = 0$ as

$$\lambda_{\mathrm{H}} = \frac{a^2(\kappa - \beta/2N\epsilon)^2 - 4\pi^2}{4h\pi^2}. \tag{S65}$$

Finally, let us briefly explain the magnitude of each physical quantity used in our numerical calculations. As claimed earlier, $\overline{K}$ and $\widetilde{K}$ are additive and subtractive coupling terms for the nematic elastic modulus, and their magnitudes are $\sim 10^{-12}$ N [6]. The coefficient h for the polarization gradient term is in the order of $\sim 10^{-10}$ J·m^3·C^{-2}, which was used in our previous work [7]. τ_1 and τ_2 are phenomenological coefficients in the Landau energy terms. They are set to be -10^3 J·m·C^{-2} and 9.88×10^5 J·m^5·C^{-4} respectively so that the equilibrium polarization strength is 4.5 μC·cm^{-2}. The value of γ is 10^{-4} V, which is reported in a recent work [8]. β is set to be of the order of 10^{-4} as mentioned before [3]. Under this condition, the amount of space charge accumulated per unit volume is estimated as $\beta \int \nabla \cdot \mathbf{P}\ dV_{\mathrm{unit}} \approx 10^{-17}$ C when $P_0 = 6$ μC·cm^{-2}, which is comparable to the reported value in ref. 3. The effective dielectric constant ε for the NF LCs is very large [9], so we set it in the order of $\sim 10^{-7}$ F·m^{-1}(The vacuum dielectric constant is 8.85×10^{-12}F·m^{-1}). The magnitude of the surface anchoring factor W_{Q} and W_{P} is set to be $\sim 10^{-6}$ J·m^{-2} [10].

Reference

1. Y. Zou and S. Aya, 2024, *arxiv preprint*, arXiv:2401.17529.
2. P. Chandra and P. B. Littlewood, in *Physics of Ferroelectrics: A Modern Perspective*, Springer Berlin Heidelberg, Berlin, Heidelberg2007, pp. 69-116.
3. K. Perera, R. Saha, P. Nepal, R. Dharmarathna, M. S. Hossain, M. Mostafa, A. Adaka, R. Waroquet, R. J. Twieg and A. Jákli, *Soft Matter*, 2023, **19**, 347-354.
4. E. Zavvou, M. Klasen-Memmer, A. Manabe, M. Bremer and A. Eremin, *Soft Matter*, 2022, **18**, 8804-8812.
5. J.-B. Lee, R. A. Pelcovits and R. B. Meyer, *Physical Review E*, 2007, **75**, 051701.
6. P.-G. De Gennes and J. Prost, *The physics of liquid crystals*, Oxford university press1993.
7. J. Zhou, Y. Zou, J. Li, M. Huang and S. Aya, *PNAS Nexus*, 2023, **2**.
8. N. Sebastián, L. Cmok, R. J. Mandle, M. R. de la Fuente, I. Drevenšek Olenik, M. Čopič and A. Mertelj, *Physical Review Letters*, 2020, **124**, 037801.
9. J. Li, H. Nishikawa, J. Kougo, J. Zhou, S. Dai, W. Tang, X. Zhao, Y. Hisai, M. Huang and S. Aya, *Science Advances*, 2021, **7**, eabf5047.
10. B. Basnet, M. Rajabi, H. Wang, P. Kumari, K. Thapa, S. Paul, M. O. Lavrentovich and O. D. Lavrentovich, *Nature Communications*, 2022, **13**, 3932.